Parallel magnetic resonance imaging reconstruction algorithm by 3-dimension directional Haar tight framelet regularization

Yan-Ran Li[a] and Xiaosheng Zhuang[b]

[a]College of Computer Science and Software Engineering, Shenzhen University, Shenzhen, 518060, P. R. China.
[b]Department of Mathematics, City University of Hong Kong, Tat Chee Avenue, Kowloon Tong, Hong Kong

ABSTRACT

In this paper, a 3-dimension *directional Haar tight framelet* (3DHF) is used to detect the related features between coil images in parallel magnetic resonance imaging (pMRI). Such a Haar tight framelet has an extremely simple geometric structure in the sense that all the high-pass filters in its underlying filter bank have only two nonzero coefficients with opposite signs. A pMRI optimization model, which we coined 3DHF-SPIRiT, by regularizing the 3DHF features on the 3-D coil image data is proposed to reduce the aliasing artifacts caused by the downsampling operation in the k-space (Fourier) domain, which can be solved by alternating direction method of multipliers (ADMM) scheme. Numerical experiments are provided to demonstrate the superiority and efficiency of our 3DHF-SPIRiT model.

Keywords: pMRI, directional Haar tight framelets, 3-D regularization, SENSE, GRAPPA, SPIRiT, ADMM.

1. INTRODUCTION

Magnetic Resonance Imaging (MRI) technique can visualize in-vivo structures without damaging radiation, but its imaging time is relatively long [21]. To accelerate imaging speed, parallel MRI (pMRI) system using an array of surface coils is proposed to simultaneously receive partial information of target slice, and only acquires parts of the k-space data of each receiver [6]. A lot of pMRI image reconstruction methods from the undersampled data have been studied and produced over the last two decades. The *sensitivity encoding* (SENSE) [22] and the *generalized autocalibrating partially parallel acquisitions* (GRAPPA) [8] are the most well-known parallel imaging techniques for reconstruction and commercially available for clinical purposes, but they provide aliased reconstructed images with artifacts when the accelerated rate is high.

To regularize the pMRI problem for SENSE-based or GRAPPA-based methods, 2-D redundant transform systems are utilized to decompose images and shrink the feature coefficients [18, 20, 24]. Using regularization on SENSE-based reconstruction model, e.g., the TV (Total Variation)-based [17, 25] or wavelet-based [3] regularization, edges can be preserved and the noise or artifacts can be removed or suppressed. Regarding edge preservation or detection, wavelets/framelets with directionality, e.g., [1, 2, 9, 14–16], have been shown to be important in such scenarios. In fact, recently, a 2-D directional Haar framelet (DHF) system is constructed with ability to detect edges of an image in the horizontal, vertical, and $\pm 45^\circ$ directions, which is successfully applied to pMRI problem [18] (see also [13]) using the SENSE-based method. However, SENSE-based methods require accurate estimation of *coil sensitivity*, which is difficult to determine due to the complex geometry of the coils. Unlike SENSE-based methods, GRAPPA [8] considers the pMRI reconstruction as an interpolation problem in the k-space domain and supposes the missing k-space coefficients can be predicted by the linear combination of its neighbour cuboid data. Though coil sensitivity is not needed for GRAPPA-based methods, they require the *auto calibration signal* (ACS) data, fully sampled at the center of the k-space, to estimate the interpolation coefficients. Regularization on calibration kernel and jointly sparse reconstructed coil channel images was proposed to update the GRAPPA-based kernel and coil image iteratively [24]. The ℓ_1-SPIRiT [20] is a GRAPPA similar

Send correspondence to X. Zhuang (xzhuang7@cityu.edu.hk), Phone: +852 3442 5942. Further contact information: Y.-R. Li (lyran@szu.edu.cn).

method by applying interpolation kernel at known and unknown k-space data for arbitrary sampling patterns, and iteratively reconstructs images by regularizing coil images together using joint sparsity-promoting norm.

More precisely, suppose we have p coil k-space data $g_j, j = 1, \ldots, p$. The sampling matrix $\mathcal{P}$ is a diagonal matrix with 0 and 1 (indicating the corresponding k-space data is skipped or not) at its diagonal elements, and the collected data of each coil is denoted by $\mathcal{P}g_j$. For the GRAPPA method, every k-space coefficient of g_j can be considered as a linear combination with the data within its neighbour of g_j and the same local neighbor of other coil data. The template of the known data with respect to the target point may have different interpolating form for each coil data. We denote the interpolation kernel with the i^{th} template for the missing position of the j^{th} coil by $\kappa_j^i \in \mathbb{C}^{n_i p \times 1}$, where n_i is the size of the known data in the 2-D template around the missing position of $g_j, j = 1, \ldots, p$. The interpolation kernels κ_j^i are estimated according to the sampling model by using the ACS data, fully sampled at the region of the center of k-space. For the j^{th} coil, we construct a matrix D_j^i by collecting the known data of the i^{th} template from ACS k-space data of p coils and denote its corresponding target data as a vector b_j^i, and then the kernel κ_j^i is estimated as

$$\min_{\kappa_j^i} \|D_j^i \kappa_j^i - b_j^i\|_2^2, \quad i = 1, \ldots, m; j = 1, \ldots, p. \tag{1}$$

where m is the number of kernels determined by the sampling model for each coil.

When the interpolation kernels κ_j^i are available, the missing coefficients can be predicted by its linear combination. Just as the coil sensitivity in the SENSE method, the kernel is also difficult to be estimated accurately even when a full k-space data is given. Moreover, the number of kernel templates could be huge especially for the random sampling model in the k-space. To reduce the number of interpolation kernels and reconstruct image from arbitrary sampling patterns in k-space, the *iterative self-consistent parallel imaging reconstruction* (SPIRiT) [19] method is proposed to estimate one interpolation kernel for each coil and reconstruct the coil images by 2D-wavelet regularization (ℓ_1-SPIRiT) [20]. The data within the cuboid, except for the target position, are all linearly combined together to predict the information in ℓ_1-SPIRiT meothod. Let the interpolating window for each coil be of size $n_1 \times n_2$, and the j^{th} coil interpolation kernel denoted by $\kappa_j \in \mathbb{C}^{(n_1 n_2 p - 1) \times 1}$ be estimated as

$$\min_{\kappa_j} \|D_j \kappa_j - b_j\|_2^2, \quad j = 1, \ldots, p, \tag{2}$$

where D_j and b_j are the known data and target interpolated data from the ACS lines, respectively.

Once such kernels κ_j are estimated, the ℓ_1-SPIRiT method utilizes the 2D-wavelet regularization for reconstructing the target slice data u. In fact, let a matrix C_j represent the j^{th} pre-estimated kernel κ_j and

$$C := \begin{bmatrix} C_1 \\ \vdots \\ C_p \end{bmatrix}, \; Q_p := \begin{bmatrix} I - \mathcal{P} & & \\ & \ddots & \\ & & I - \mathcal{P} \end{bmatrix}, \; \mathcal{F}_p := \begin{bmatrix} \mathcal{F} & & \\ & \ddots & \\ & & \mathcal{F} \end{bmatrix}, \; g := \begin{bmatrix} \mathcal{P}g_1 \\ \vdots \\ \mathcal{P}g_p \end{bmatrix}, \; W_{2D} := \begin{bmatrix} W \\ \vdots \\ W \end{bmatrix}. \tag{3}$$

Here, I is the identity matrix, $\mathcal{F}$ is the *discrete Fourier transform* matrix with inverse $\mathcal{F}^{-1}$, and W corresponds to a 2-D wavelet transform associated with certain wavelet/framelet system. The optimization model by ℓ_1-SPIRiT [20] is then presented by

$$\min_u \left\{ \frac{1}{2} \|(C - I)(Q_p u + g)\|_2^2 + \lambda \|W_{2D} \mathcal{F}_p^{-1} (Q_p u + g)\|_{1,2} \right\}, \tag{4}$$

where λ is the regularization parameter, and $\|W_{2D} \mathcal{F}_p^{-1} (Q_p u + g)\|_{1,2}$ is the sparsity-promoting term.

Note that each coil image is decomposed by the 2-D wavelet/framelet transform, the relationship between coils is not considered for regularization. The W_{2D} in both the SENSE-based model in [18] and the above model (4) only utilizes 2-D coil image information independently while ignoring the correlated information among multi-coil images. In fact, The coil images stacked together can be considered as 3-D cuboid data and their related features can be regularized by the 3-D tight framelet systems to reduce the aliasing artifacts. In view of this,

a modified version of (4) using 3-D directional Haar tight framelet (3DHF) regularization model for pMRI is proposed as:

$$\min_u \left\{ \frac{1}{2}\|(C-I)(Q_p u+g)\|_2^2 + \lambda \|W_{3D}\mathcal{F}_p^{-1}(Q_p u+g)\|_1 \right\} \tag{5}$$

where W_{3D} in this paper is a framelet transfrom associated with the 3-D directional Haar tight framelet. We coined such a model 3DHF-SPIRiT, which can be solve by the ADMM scheme [7]. We next introduce the 3-D directional Haar tight framelet associated with W_{3D}.

2. DIRECTIONAL HAAR TIGHT FRAMELETS

In this section, we introduce compactly supported tight framelets with directionality and very simple geometric structures from the Haar refinable functions. All the high-pass filters in such directional Haar tight framelets have only two nonzero coefficients with oppositive signs. Consequently, all of them naturally exhibit directionality and their associated fast framelet transforms can be efficiently implemented through simple difference operations.

Tight framelets are closely related to filter banks. Before proceeding to their connections, let us recall some definitions and notation first. By $L_2(\mathbb{R}^d)$, we denote the usual space of square integrable functions defined on $\mathbb{R}^d$. Let $\phi, \psi_1, \ldots, \psi_s \in L_2(\mathbb{R}^d)$. We say that $\{\phi; \psi_1, \ldots, \psi_s\}$ is *a (nonhomogeneous dyadic) tight framelet in* $L_2(\mathbb{R}^d)$ if $\|f\|^2_{L_2(\mathbb{R}^d)} = \sum_{k\in\mathbb{Z}^d} |\langle f, \phi(\cdot - k)\rangle|^2 + \sum_{j=0}^{\infty}\sum_{\ell=1}^{s}\sum_{k\in\mathbb{Z}^d} |\langle f, 2^{jd/2}\psi_\ell(2^j\cdot - k)\rangle|^2$, $\forall\, f \in L_2(\mathbb{R}^d)$. By $l_0(\mathbb{Z}^d)$ we denote the set of all finitely supported sequences/filters $a = \{a(k)\}_{k\in\mathbb{Z}^d} : \mathbb{Z}^d \to \mathbb{C}$ on $\mathbb{Z}^d$. For a filter $a \in l_0(\mathbb{Z}^d)$, its *Fourier series* is defined to be $\widehat{a}(\xi) := \sum_{k\in\mathbb{Z}^d} a(k)e^{-\mathrm{i}k\cdot\xi}$ for $\xi \in \mathbb{R}^d$, which is a $2\pi\mathbb{Z}^d$-periodic trigonometric polynomial. In particular, by $\boldsymbol{\delta}$ we denote the *Dirac sequence* such that $\boldsymbol{\delta}(0) = 1$ and $\boldsymbol{\delta}(k) = 0$ for all $k \in \mathbb{Z}^d\backslash\{0\}$. For $\gamma \in \mathbb{Z}^d$, we also use the notation $\boldsymbol{\delta}_\gamma$ to stand for the sequence $\boldsymbol{\delta}(\cdot - \gamma)$, i.e., $\boldsymbol{\delta}_\gamma(\gamma) = 1$ and $\boldsymbol{\delta}_\gamma(k) = 0$ for all $k \in \mathbb{Z}^d\backslash\{\gamma\}$. Note that $\widehat{\boldsymbol{\delta}_\gamma}(\xi) = e^{-\mathrm{i}\gamma\cdot\xi}$. For filters $a, b_1, \ldots, b_s \in l_0(\mathbb{Z}^d)$, we say that a filter bank $\{a; b_1, \ldots, b_s\}$ is *a (d-dimensional dyadic) tight framelet filter bank* if

$$\widehat{a}(\xi)\overline{\widehat{a}(\xi+\pi\omega)} + \sum_{\ell=1}^{s} \widehat{b_\ell}(\xi)\overline{\widehat{b_\ell}(\xi+\pi\omega)} = \boldsymbol{\delta}(\omega),\ \forall\, \xi \in \mathbb{R}^d, \omega \in \{0,1\}^d. \tag{6}$$

Equation (6) is just the *perfect reconstruction property* of a tight framelet filter bank ([12, Theorems 1.1.1 and 1.1.4]). When $\omega = 0$ in (6), it is the *partition of unity* condition:

$$|\widehat{a}(\xi)|^2 + \sum_{\ell=1}^{s} |\widehat{b_\ell}(\xi)|^2 = 1,\ \forall\, \xi \in \mathbb{R}^d. \tag{7}$$

Let $a, b_1, \ldots, b_s \in l_0(\mathbb{Z}^d)$ and assume that $\widehat{a}(0) = \sum_{k\in\mathbb{Z}^d} a(k) = 1$. Then we can define compactly supported tempered distributions ϕ and $\psi_1, \ldots, \psi_s$ on $\mathbb{R}^d$ through $\widehat{\phi}(\xi) := \prod_{j=1}^{\infty} \widehat{a}(2^{-j}\xi)$ and $\widehat{\psi_\ell}(\xi) = \widehat{b_\ell}(\xi/2)\widehat{\phi}(\xi/2)$, $\xi \in \mathbb{R}^d, \ell = 1, \ldots, s$. It is known in [11, Corollary 12 and Theorem 17] and [12, Theorem 4.5.4] that $\{\phi; \psi_1, \ldots, \psi_s\}$ is a tight framelet in $L_2(\mathbb{R}^d)$ if and only if $\{a; b_1, \ldots, b_s\}$ is a tight framelet filter bank. Also c.f. [4, 5, 10, 23] for related results. The tempered distribution ϕ is called *a refinable function* satisfying the refinement equation $\widehat{\phi}(\xi) = \widehat{a}(\xi/2)\widehat{\phi}(\xi/2)$ for $\xi \in \mathbb{R}^d$ with the refinement filter a. In fact, it is known in [12, Theorem 4.5.4] that every tight framelet $\{\phi; \psi_1, \ldots, \psi_s\}$ in $L_2(\mathbb{R}^d)$ must come from a generalized tight framelet filter bank $\{a; b_1, \ldots, b_s\}$ through the refinable structure. Consequently, in this paper we mainly focus on tight framelet filter banks.

Motivated by [18], the authors in [13] prove the following theorem.

THEOREM 2.1. *Let* $a^H = 2^{-d}\sum_{\gamma\in\{0,1\}^d} \boldsymbol{\delta}_\gamma$ *be the d-dimensional Haar low-pass filter. Define the high-pass filters* $b_1, \ldots, b_s$ *with* $s := \binom{2^d}{2} = 2^{d-1}(2^d - 1)$ *in the following way:* $2^{-d}(\boldsymbol{\delta}_{\gamma_1} - \boldsymbol{\delta}_{\gamma_2})$ *for all undirected edges with endpoints* $\gamma_1, \gamma_2 \in \{0,1\}^d$ *and* $\gamma_1 \neq \gamma_2$. *Then* $\{a^H; b_1, \ldots, b_s\}$ *is a tight framelet filter bank such that all the high-pass filters* $b_1, \ldots, b_s$ *have directionality and exhibit* $\frac{1}{2}(3^d - 1)$ *directions in dimension d. Define functions* ϕ *and* $\psi_1, \ldots, \psi_s$ *through* $\widehat{\phi}(\xi) := \prod_{j=1}^{\infty} \widehat{a}(2^{-j}\xi)$ *and* $\widehat{\psi_\ell}(\xi) = \widehat{b_\ell}(\xi/2)\widehat{\phi}(\xi/2)$, $\xi \in \mathbb{R}^d, \ell = 1, \ldots, s$. *Then* $\{\phi; \psi_1, \ldots, \psi_s\}$ *is a d-dimensional directional compactly supported Haar tight framelet in* $L_2(\mathbb{R}^d)$.

When $d = 1$, the tight framelet filter bank in Theorem 2.1 is just the standard *Haar orthogonal wavelet filter bank* $\mathrm{DHF}_1 := \{a^H; b\}$ with $a^H = \frac{1}{2}(\boldsymbol{\delta}_0 + \boldsymbol{\delta}_1)$ and $b = \frac{1}{2}(\boldsymbol{\delta}_0 - \boldsymbol{\delta}_1)$.

When $d = 2$, Theorem 2.1 recovers the *2-D directional Haar tight framelet filter bank* $\mathrm{DHF}_2 := \{a^H; b_1, \ldots, b_6\}$ in [18] with $a^H = \frac{1}{4}(\boldsymbol{\delta}_{(0,0)} + \boldsymbol{\delta}_{(0,1)} + \boldsymbol{\delta}_{(1,0)} + \boldsymbol{\delta}_{(1,1)})$ and

$$b_1 = \frac{1}{4}(\boldsymbol{\delta}_{(0,0)} - \boldsymbol{\delta}_{(0,1)}), \quad b_2 = \frac{1}{4}(\boldsymbol{\delta}_{(0,0)} - \boldsymbol{\delta}_{(1,0)}), \quad b_3 = \frac{1}{4}(\boldsymbol{\delta}_{(0,0)} - \boldsymbol{\delta}_{(1,1)}),$$
$$b_4 = \frac{1}{4}(\boldsymbol{\delta}_{(0,1)} - \boldsymbol{\delta}_{(1,0)}), \quad b_5 = \frac{1}{4}(\boldsymbol{\delta}_{(0,1)} - \boldsymbol{\delta}_{(1,1)}), \quad b_6 = \frac{1}{4}(\boldsymbol{\delta}_{(1,0)} - \boldsymbol{\delta}_{(1,1)}).$$

When $d = 3$, Theorem 2.1 gives rise to the following *3-D directional Haar tight framelet filter bank* $\mathrm{DHF}_3^1 := \{a^H; b_1, \ldots, b_{28}\}$ with $a^H = \frac{1}{8}(\boldsymbol{\delta}_{(0,0,0)} + \boldsymbol{\delta}_{(0,0,1)} + \boldsymbol{\delta}_{(0,1,0)} + \boldsymbol{\delta}_{(0,1,1)} + \boldsymbol{\delta}_{(1,0,0)} + \boldsymbol{\delta}_{(1,0,1)} + \boldsymbol{\delta}_{(1,1,0)} + \boldsymbol{\delta}_{(1,1,1)})$ and

$$b_1 = \frac{1}{8}(\boldsymbol{\delta}_{(0,0,0)} - \boldsymbol{\delta}_{(0,0,1)}), \quad b_2 = \frac{1}{8}(\boldsymbol{\delta}_{(0,0,0)} - \boldsymbol{\delta}_{(0,1,0)}), \quad b_3 = \frac{1}{8}(\boldsymbol{\delta}_{(0,0,0)} - \boldsymbol{\delta}_{(0,1,1)}), \quad b_4 = \frac{1}{8}(\boldsymbol{\delta}_{(0,0,0)} - \boldsymbol{\delta}_{(1,0,0)}),$$
$$b_5 = \frac{1}{8}(\boldsymbol{\delta}_{(0,0,0)} - \boldsymbol{\delta}_{(1,0,1)}), \quad b_6 = \frac{1}{8}(\boldsymbol{\delta}_{(0,0,0)} - \boldsymbol{\delta}_{(1,1,0)}), \quad b_7 = \frac{1}{8}(\boldsymbol{\delta}_{(0,0,0)} - \boldsymbol{\delta}_{(1,1,1)}), \quad b_8 = \frac{1}{8}(\boldsymbol{\delta}_{(0,0,1)} - \boldsymbol{\delta}_{(0,1,0)}),$$
$$b_9 = \frac{1}{8}(\boldsymbol{\delta}_{(0,0,1)} - \boldsymbol{\delta}_{(0,1,1)}), \quad b_{10} = \frac{1}{8}(\boldsymbol{\delta}_{(0,0,1)} - \boldsymbol{\delta}_{(1,0,0)}), \quad b_{11} = \frac{1}{8}(\boldsymbol{\delta}_{(0,0,1)} - \boldsymbol{\delta}_{(1,0,1)}), \quad b_{12} = \frac{1}{8}(\boldsymbol{\delta}_{(0,0,1)} - \boldsymbol{\delta}_{(1,1,0)}),$$
$$b_{13} = \frac{1}{8}(\boldsymbol{\delta}_{(0,0,1)} - \boldsymbol{\delta}_{(1,1,1)}), \quad b_{14} = \frac{1}{8}(\boldsymbol{\delta}_{(0,1,0)} - \boldsymbol{\delta}_{(0,1,1)}), \quad b_{15} = \frac{1}{8}(\boldsymbol{\delta}_{(0,1,0)} - \boldsymbol{\delta}_{(1,0,0)}), \quad b_{16} = \frac{1}{8}(\boldsymbol{\delta}_{(0,1,0)} - \boldsymbol{\delta}_{(1,0,1)}),$$
$$b_{17} = \frac{1}{8}(\boldsymbol{\delta}_{(0,1,0)} - \boldsymbol{\delta}_{(1,1,0)}), \quad b_{18} = \frac{1}{8}(\boldsymbol{\delta}_{(0,1,0)} - \boldsymbol{\delta}_{(1,1,1)}), \quad b_{19} = \frac{1}{8}(\boldsymbol{\delta}_{(0,1,1)} - \boldsymbol{\delta}_{(1,0,0)}), \quad b_{20} = \frac{1}{8}(\boldsymbol{\delta}_{(0,1,1)} - \boldsymbol{\delta}_{(1,0,1)}),$$
$$b_{21} = \frac{1}{8}(\boldsymbol{\delta}_{(0,1,1)} - \boldsymbol{\delta}_{(1,1,0)}), \quad b_{22} = \frac{1}{8}(\boldsymbol{\delta}_{(0,1,1)} - \boldsymbol{\delta}_{(1,1,1)}), \quad b_{23} = \frac{1}{8}(\boldsymbol{\delta}_{(1,0,0)} - \boldsymbol{\delta}_{(1,0,1)}), \quad b_{24} = \frac{1}{8}(\boldsymbol{\delta}_{(1,0,0)} - \boldsymbol{\delta}_{(1,1,0)}),$$
$$b_{25} = \frac{1}{8}(\boldsymbol{\delta}_{(1,0,0)} - \boldsymbol{\delta}_{(1,1,1)}), \quad b_{26} = \frac{1}{8}(\boldsymbol{\delta}_{(1,0,1)} - \boldsymbol{\delta}_{(1,1,0)}), \quad b_{27} = \frac{1}{8}(\boldsymbol{\delta}_{(1,0,1)} - \boldsymbol{\delta}_{(1,1,1)}), \quad b_{28} = \frac{1}{8}(\boldsymbol{\delta}_{(1,1,0)} - \boldsymbol{\delta}_{(1,1,1)}).$$

See Figure 1 for the illustration of the filter banks $\mathrm{DHF}_1, \mathrm{DHF}_2$, and DHF_3^1.

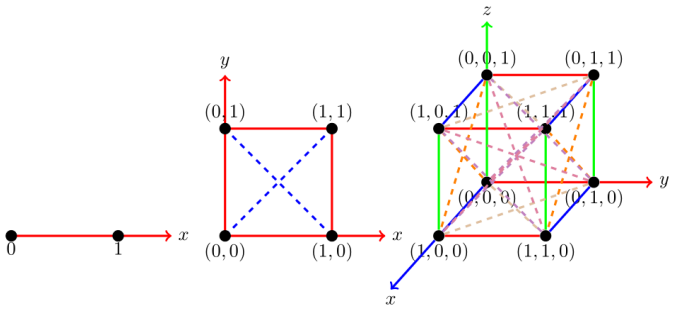

Figure 1. Directional Haar tight framelet filter banks in $d = 1, 2, 3$ respectively, where each line connecting two vertices $\gamma_1, \gamma_2 \in \{0, 1\}^d$ represents a high-pass filter $b_\ell := 2^{-d}(\boldsymbol{\delta}_{\gamma_1} - \boldsymbol{\delta}_{\gamma_2})$.

In this paper, we focus on $d = 3$ since the pMRI data are formed by stacking a sequence of 2-D pMRI coil-images as a 3-D signal. Moreover, we aim at reconstructing signal from its degenerated version, where for such tasks, redundant representation systems are more favour since it provides more information for data recovery. Furthermore, in signal/image processing, translation in-variance property of a discrete transform is very much desirable especially in the scenario of signal denoising/inpainting. To preserve the translation in-variance property, in this paper, we hence use the more redundant version of the discrete framelet transform, that is, the *undecimated discrete framelet transforms* (UDFmT):

$$\text{Decompoistion:} \quad v_{j-1} = v_j * (a^\star \uparrow 2^{J-j}), \quad w_{j-1;\ell} = v_j * (b_\ell^\star \uparrow 2^{J-j}), \quad \ell = 1, \ldots, s, \quad j = J, \ldots, 1.$$

$$\text{Reconstruciton:} \quad v_j = v_{j-1} * (a \uparrow 2^{J-j}) + \sum_{\ell=1}^{s} w_{j-1;\ell} * (b_\ell \uparrow 2^{J-j}), \quad j = 1, \ldots, J,$$

where $*$ is the *convolution* operation and $\uparrow m$ is the *upsampling* operation.

For undecimated discrete framelet transforms, we only need the filter bank satisfying the *partition of unity condition* as in (7). Consequently, filters up to a translation indeed represent the same feature of input data, which can then be regrouped together. In $\text{DHF}_3^1 = \{a^H; b_1, \ldots, b_{28}\}$, there are many filters characterizing the same directional property. For example, the filters in $\{b_1, b_{14}, b_{23}, b_{28}\}$ represent the same z-direction (vertical), the filters in $\{b_2, b_9, b_{25}, b_{27}\}$ represent the same y-direction, etc. In view of this, the above 28 high-pass filters can actually be regrouped to 13 filters as a filter bank $\text{DHF}_3^2 := \{a^H; b_x, b_y, b_z, b_{xy}, b_{x,y}, b_{xz}, b_{x,z}, b_{yz}, b_{y,z}, b_{xyz}, b_{xy,z}, b_{x,yz}, b_{xz,y}\}$:

$$
\begin{aligned}
b_x &= \frac{1}{4}(\boldsymbol{\delta}_{(1,0,0)} - \boldsymbol{\delta}_{(0,0,0)}), & b_y &= \frac{1}{4}(\boldsymbol{\delta}_{(0,1,0)} - \boldsymbol{\delta}_{(0,0,0)}), & b_z &= \frac{1}{4}(\boldsymbol{\delta}_{(0,0,1)} - \boldsymbol{\delta}_{(0,0,0)}),\\
b_{xy} &= \frac{\sqrt{2}}{8}(\boldsymbol{\delta}_{(1,1,0)} - \boldsymbol{\delta}_{(0,0,0)}), & b_{x,y} &= \frac{\sqrt{2}}{8}(\boldsymbol{\delta}_{(1,0,0)} - \boldsymbol{\delta}_{(0,1,0)}), & b_{xz} &= \frac{\sqrt{2}}{8}(\boldsymbol{\delta}_{(1,0,1)} - \boldsymbol{\delta}_{(0,0,0)}),\\
b_{x,z} &= \frac{\sqrt{2}}{8}(\boldsymbol{\delta}_{(1,0,0)} - \boldsymbol{\delta}_{(0,0,1)}), & b_{yz} &= \frac{\sqrt{2}}{8}(\boldsymbol{\delta}_{(0,1,1)} - \boldsymbol{\delta}_{(0,0,0)}), & b_{y,z} &= \frac{\sqrt{2}}{8}(\boldsymbol{\delta}_{(0,1,0)} - \boldsymbol{\delta}_{(0,0,1)}),\\
b_{xyz} &= \frac{1}{8}(\boldsymbol{\delta}_{(1,1,1)} - \boldsymbol{\delta}_{(0,0,0)}), & b_{xy,z} &= \frac{1}{8}(\boldsymbol{\delta}_{(1,1,0)} - \boldsymbol{\delta}_{(0,0,1)}), & b_{x,yz} &= \frac{1}{8}(\boldsymbol{\delta}_{(1,0,0)} - \boldsymbol{\delta}_{(0,1,1)}),\\
b_{xz,y} &= \frac{1}{8}(\boldsymbol{\delta}_{(1,0,1)} - \boldsymbol{\delta}_{(0,1,0)}).
\end{aligned}
$$

See Figure 2 for its illustration. In our processing of the output framelet coefficient sequences, information involving the z-filters, i.e., those b_z, b_{xz}, b_{xyz}, etc., are actually 'bad' features for our 3-D signal reconstruction. In fact, they represent local contrast discrepancy between coil images which does not play a role in our restriction process. We thus ignore the processing for the output coefficient sequences related to those z-filters. The W_{3D} in (5) is then the UDFmT-decomposition process associated with DHF_3^2 while W_{3D}^T is the UDFmT-reconstruction process associated with DHF_3^2.

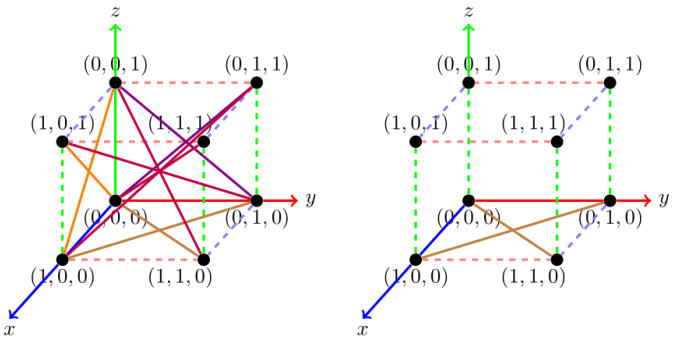

Figure 2. Directional Haar tight framelet filter banks in $\text{DHF}_3^2 := \{a^H; b_x, b_y, b_z, b_{xy}, b_{x,y}, b_{xz}, b_{x,z}, b_{yz}, b_{y,z}, b_{xyz}, b_{xy,z}, b_{x,yz}, b_{xz,y}\}$ (solid edges in $\{0,1\}^3$).

3. NUMERICAL EXPERIMENTS

In this section, we illustrate the superiority and efficiency of our 3DHF-SPIRiT model (5) comparing to the ℓ_1-SPIRiT model (4). Note that both models can be solved by using ADMM method [7].

The source code of ℓ_1-SPIRiT [20] method can be downloaded from the web site of one of the authors*. Four phantom MR images are acquired on a 3T MRI System (Tim Trio, Siemens, Erlangen, Germany), which are T_2-weighted images acquired by a turbo spin-echo sequence. The detailed imaging parameters are set as follows: field of view (FOV) = 256×256 mm^2, image marix size = 512×512, slice thicknesses (ST) = 3 mm, flip angle = 180 degree, repetition time (TR) = 4000 ms, echo time (TE) = 71 ms, echo train length (ETL) = 11 and number of excitation (NEX) = 1. Figures 3 (a)–(d) are four coil MR images without uniform intensity by the

*The code is available at: http://www.eecs.berkeley.edu/~mlustig/Software.html

full k-space data, and their *sum of square* (SoS) image is shown in Figure 4 (a). Though some parts of each coil image are lighter and others are darker, the SoS image by each coil image is harmony intensity with clear edges.

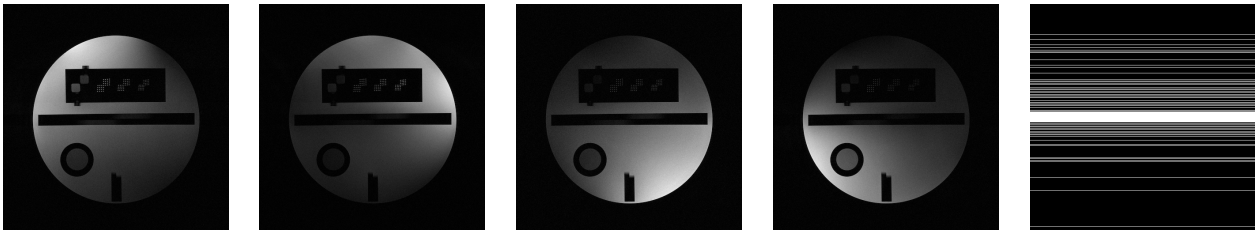

(a) (b) (c) (d) (e)

Figure 3. (a)–(d) Four coil images by the full k-space; (e) Sampling model of 15% k-space with 24 ACS lines.

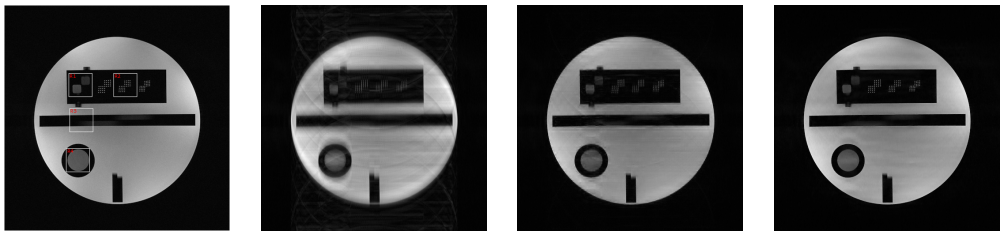

(a) (b) (c) (d)

Figure 4. Reconstruction results on 15% k-space data. (a) SoS image of the full k-space with zoom-in parts displayed in Figure 5; (b) SoS image of the 15% k-space data; (c) ℓ_1-SPIRiT [20] with parameter 0.009; (d) Our 3DHF-SPIRiT.

The coil images in Figures 3 (a)–(d) can be considered as parts of information of the target imaging slice, and are redundant with each others. Thus parts of each coil k-space data are collected to fuse a desired image and to accelerate the imaging speed. An example with four coil images of size 512×512 is adopted in this experiment using coil pseudo random downsampling k-space data in the phase-encoding direction on the Cartesian coordinate. According to the sampling model in Figure 3 (e) with 24 ACS lines in the center of k-space, about 15% of k-space data (marked by white color there) of each coil are collected for shortening imaging time. Figure 4 (b) is the SoS image of the coil images obtained by applying the inverse Fourier transform for the collected k-space data with zero-padding for missing data. It has aliasing artifacts obviously and is blurry with unclear edges.

The ℓ_1-SPIRiT method [20] and our proposed 3DHF-SPIRiT method are with the calibration kernel size of 11-by-11 for each coil k-space data, which are used to reconstruct an image from four coil images with the sampling model described in Figure 3 (e). The SoS image of the full k-space is considered as a reference image shown in Figure 4 (a). The image in Figure 4 (c) is the result from the ℓ_1-SPIRiT using the default settings in the source code of ℓ_1-SPIRiT algorithm except that the regularization parameter is set to be 0.009 after an extensive trial-and-error search to find the best one. The reconstructed image by our 3DHF-SPIRiT is shown in Figure 4 (d). Clearly, aliasing artifacts appeared in Figure 4 (b) are significantly suppressed by the two methods. But the aliasing artifacts in the image by ℓ_1-SPIRiT is more obvious than that in the image by our 3DHF-SPIRiT.

To further evaluate the quality of the reconstructions, four regions shown in Figure 4 (a) are zoomed in Figure 5. For the 'R1' region, The surface of two squares reconstructed by ℓ_1-SPIRiT has little artifact, but our 3DHF-SPIRiT can remove this artifact and retrieve the shape of the left-down square more close to reference one. For the 'R2' region in the second row of Figure 4, the dots by our 3DHF-SPIRiT are *sharper* and *brighter*, which are close to dots by SoS image of the full k-space, but those by ℓ_1-SPIRiT is blurred and can not be separated with each other. For the 'R3' and 'R4' regions, our 3DHF-SPIRiT is still efficient to keep edges and remove artifacts as well as perform much better than the ℓ_1-SPIRiT. We conclude that our 3DHF-SPIRiT performs superiorly in preserving the details of the images and removing noisy artifacts in smooth area, and provide high-quality MRI images.

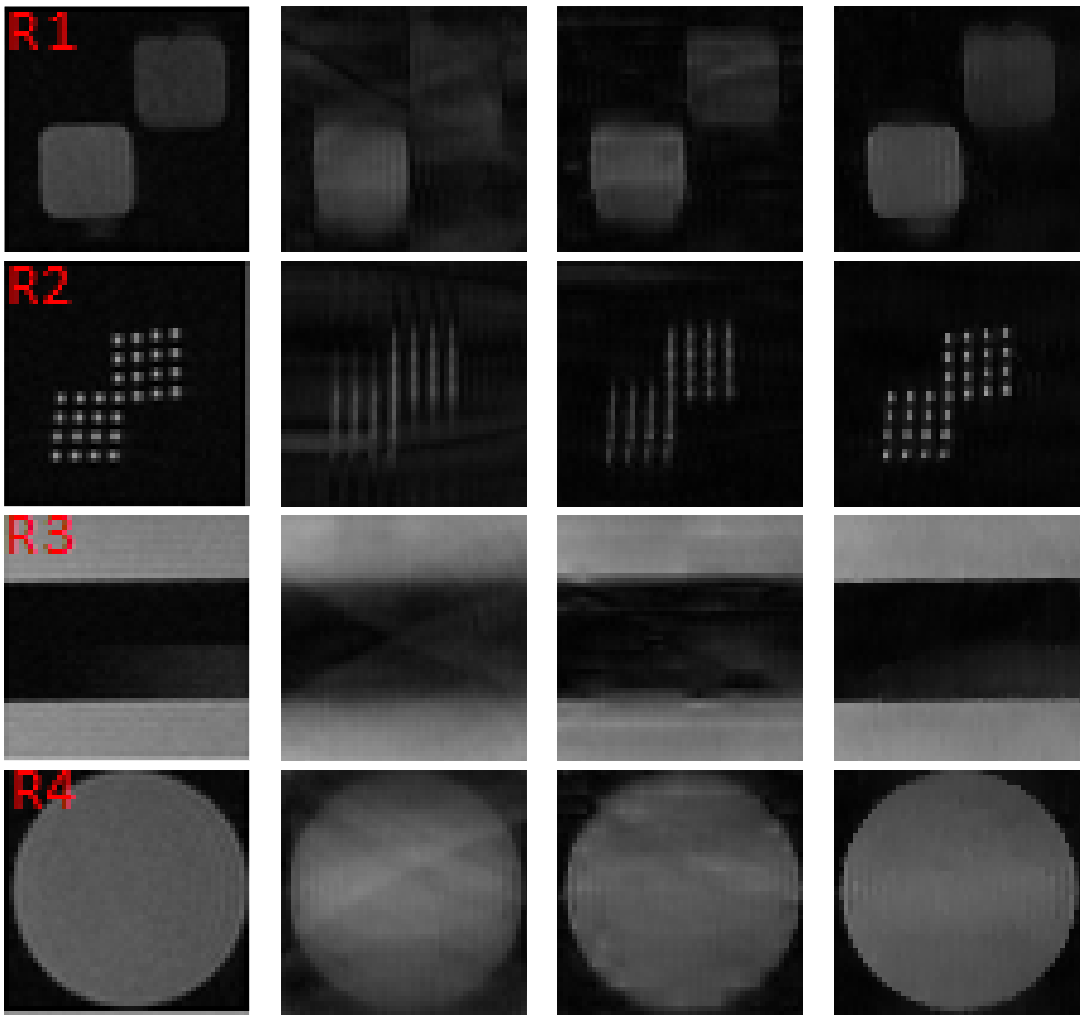

(a) (b) (c) (d)

Figure 5. Zoom-in parts of Figure 4. (a) SoS image of the full k-space with zoom-in parts. (b) SoS image of the 15% k-space data. (c) ℓ_1-SPIRiT [20] with parameter 0.009. (d) Our 3DHF-SPIRiT with parameter 0.02.

ACKNOWLEDGMENTS

The research of Y.-R. Li and the work described in this paper was partially supported by Shenzhen R&D Program (JCYJ20180305124325555) and "Shenzhen Institute of Artificial Intelligence and Robotics for Society". The research of X. Zhuang and the work described in this paper was partially supported by a grant from the Research Grants Council of the Hong Kong Special Administrative Region, China (Project No. CityU 11302218).

REFERENCES

[1] Bodmann B. G., Kutyniok G., and Zhuang X., "Gabor shearlets," *Applied and Computational Harmonic Analysis* 38(1), 87–114 (2015).

[2] Candès E. J. and Donoho D. L., "New tight frames of curvelets and optimal representations of objects with piecewise C^2 singularities," *Communications on Pure and Applied Mathematics* 57(2), 219–266 (2004).

[3] Chaâri L., Pesquet J. C., Benazza-Benyahia A. , and Ciuciu P. , "A wavelet-based regularized reconstruction algorithm for SENSE parallel MRI with applications to neuroimaging," *Medical Image Analysis* 12(2), 185–201 (2011).

[4] C. K. Chui, W. He, and J. Stöckler, "Compactly supported tight and sibling frames with maximum vanishing moments," *Applied and Computational Harmonic Analysis* 13(3), 224–262 (2002).

[5] Daubechies I., Han B., Ron A., and Shen Z., "Framelets: mra-based constructions of wavelet frames," *Applied and Computation Harmonic Analysis* 14(1), 1–46 (2003).

[6] Deshmane A., Gulani V., Griswold M. A., and Seiberlich N., "Parallel MR imaging," *Journal of Magnetic Resonance Imaging* 36 (1), 55–72 (2012).

[7] Gabay D. and Mercier B., "A dual algorithm for the solution of nonlinear variational problems via finite-element approximations," *Computers and Mathematics with Applications* 2(1), 17–40 (1976).

[8] Griswold M. A., Jakob P. M., Heidemann R. M., Nittka M., Jellus V., Wang J., Kiefer B., and Haase A., "Generalized autocalibrating partially parallel acquisitions (GRAPPA)," *Magnetic Resonance in Medicine* 47(6), 1202–1210 (2002).

[9] Guo K., Kutyniok G., and Labate D., "Sparse multidimensional representations using anisotropic dilation and shear operators," *Wavelets and Splines (Athens, GA, 2005), Nashboro Press, Nashville*, 189–201 (2006).

[10] Han B., "On dual wavelet tight frames," *Applied and Computational Harmonic Analysis* 4(4), 380–413 (1997).

[11] Han B., "Nonhomogeneous wavelet systems in high dimensions," *Applied and Computational Harmonic Analysis* 32(2), 169–196 (2012).

[12] Han B., *Framelets and Wavelets: Algorithms, Analysis, and Applications*. Springer International Publishing, (2018).

[13] Han B., Li T., and Zhuang X., "Directional compactly supported box spline tight framelets with simple geometric structure," *Applied Mathematics Letters* 91, 213–219 (2019).

[14] Han B. and Zhao Z., "Tensor product complex tight framelets with increasing directionality," *SIAM Journal on Imaging Sciences* 7(2), 997–1034 (2014).

[15] Han B., Zhao Z., and Zhuang X., "Directional tensor product complex tight framelets with low redundancy," *Applied and Computational Harmonic Analysis* 41(2), 603–637 (2016).

[16] Han B. and Zhuang X., "Smooth affine shear tight frames with MRA structures," *Applied and Computational Harmonic Analysis* 39(2), 300–338 (2015).

[17] Keeling S. L., Clason C., Hintermüller M., Knoll F., Laurain A., and von Winckel G., "An image space approach to Cartesian based parallel MR imaging with total variation regularization," *Medical Image Analysis* 16(1), 189–200 (2012).

[18] Li Y.-R., Chan R. H., Shen L., Hsu Y.-C., and Tseng W.-Y. I., "An adaptive directional haar framelet-based reconstruction algorithm for parallel magnetic resonance imaging," *SIAM Journal on Imaging Sciences* 9(2), 794–821 (2016).

[19] Lustig M. and Pauly J. M., "SPIRiT: iterative self-consistent parallel imaging reconstruction from arbitrary k-space," *Magnetic Resonance in Medicine* 64(2), 457–471 (2010).

[20] Murphy M., Alley M., Demmel J., Keutzer K., Vasanawala S., and Lustig M., "Fast ℓ_1-SPIRiT compressed sensing parallel imaging MRI: Scalable parallel implementation and clinically feasible runtime," *IEEE Transactions on Medical Imaging* 31(6), 1250–1262 (2012).

[21] Novelline R. A., *Squire's fundamentals of radiology*. 5th Edition, Cambridge: Harvard University Press, 1997.

[22] Pruessmann K. P., Weiger M., Scheidegger M. B., and Boesiger P., "SENSE: sensitivity encoding for fast MRI," *Magnetic Resonance in Medicine* 42(5), 952–962 (1999).

[23] Ron A. and Shen Z., "Affine system in $L_2(R^d)$: the analysis of the analysis operator," *Journal of Functional Analysis* 148, 408–447 (1997).

[24] Weller D. S., Polimeni J. R., Grady L., Wald L. L., Adalsteinsson E., and Goyal V. K., "Sparsity-promoting calibration for GRAPPA accelerated parallel MRI reconstruction," *IEEE Transactions on Medical Imaging* 32(7), 1325–1335 (2013).

[25] Ye X., Chen Y., and Huang F., "Computational acceleration for mr image reconstruction in partially parallel imaging," *IEEE Transactions on Medical Imaging*30(5), 1055–1063 (2011).